JAMJams: Jagged Anisotropic Mechanically Jamming Appendages for Robot Locomotion

Ignatius Widjaja[1] Nick Gravish[1], *Member, IEEE,*

***Abstract*— Laminate structures with nonlinear stiffness and controllable bending properties have applications as appendages for soft robot locomotion. In this paper, we develop a laminate-based structure for soft-robotics called Jagged Anisotropic Mechanically Jamming (JAMJam) sheets. JAMJam sheets are comprised of two flexible layers with rigid anisotropic structures 3D printed onto the flexible surface. The rigid elements between the flexible sheets are displaced longitudinally as the sheets are bent and when the elements make contact the bending stiffness increases and the resulting curvature can be controlled. In this work we study a simple example of a JAMJam sheet consisting of controllable bending curvature which is anisotropic along the forward and backward directions. We characterize the JAMJam behavior through force-displacement measurements and we implement the JAMJam sheets as appendages in a swimming robot. We compare the JAMJam mechanics under representative limb motions for a swimming robot and compare two types of appendages. Lastly, a robot utilizing the appendages is designed for shallow-water environments, which can both walk while semi-submerged at up to 9 cm/s and swim at 7.2 cm/s. The robot is capable of locomotion in both turf and sandy laboratory conditions, and can traverse over obstacles in its path.**

I. Introduction

Robots have revolutionized the way humans explore the natural environment, allowing for forays into environments such as space and the deep sea that are inaccessible to the humans. Innovative solutions are continually being developed to address the challenges faced by robotics in various applications, from search and rescue missions to environmental monitoring to off-world exploration [1].

However, many of these robots are environmentally invasive to the spaces they explore, and are ill-suited to unexpected changes in terrain. To counter this, interest has been generated in soft and bio-inspired robotics, which seeks to emulate the adaptability and non-intrusiveness of systems found in nature. The study of passive compliance in biological systems has offered valuable insights that can be applied to the development of robotic systems that are more adaptable and less invasive than traditional robots [2]–[12].

Much work has been conducted to design and develop bio-inspired robots which traverse difficult terrains utilizing passive compliance without traditional rotary contact such as propellers or wheels [2]. The PoseiDRONE swimming/crawling robot utilizes a crankshaft to drive, and a non-symmetric cable system to manipulate, its soft rubber-like arm [13]. Shape memory alloys further distance robots' reliance on rotary actuators, instead exploiting thermal properties to generate motion [14]. Passively retracting/extending legs on a robot enable better traversal in confined areas without sacrificing speed in unconfined areas [15].

A subsection of these passively compliant robots generate their forward motion utilizing mechanical anisotropy, allowing for simplified actuation while maintaining intended behavior [16]. Several methods of generating anisotropic forces have been studied. Square fiber structures with jamming produced by vacuum allow for programmable bending stiffness with a slender cross-section [17]. Passive joints with a return spring on a centipede-like robot enable anisotropic compliance in unstructured environments [18]. Kirigami used as a skin provides flexibility and directional friction forces for a snake-like tubular robot [19]. Multi-jointed arms with asymmetric joint constraints are the key for a digging robot to traverse and burrow in a natural sandy environment at depth [20].

A subsection of these robots then utilize underactuation to achieve their goals [21]–[23]. Multi-jointed arms with asymmetric joint constraints are the key for an underactuated digging robot to traverse and burrow in a natural sandy environment at depth [20]. The method utilized to achieve passively compliant appendages with anisotropic force generation in this paper is inspired by previous work [24], [25]. This structure allows for constrained bending of thin plates or sheets to generate pre-determined curves

In this paper a new design for a passively compliant, anisotropic, and minimally actuated appendage, the Jagged Anisotropic Mechanically Jamming (JAMJam) Appendage, is introduced. The appendage is characterized in its bending characteristics and force capabilities to understand its possible utilization in simplified robot systems for traversing terrain. One such system, the JAMJam robot, is designed for shallow water environments, with additional consideration for invertibility, ease of manufacture and system modularity. The JAMJam robot is built, tested, and characterized in laboratory conditions. Other possible robot platforms are also briefly discussed.

II. Design of JAMJam Appendage

The JAMJam appendage is designed to generate a large force when swept in one direction, forwards, and only a small force in the opposite direction of motion, backwards. This mechanical anisotropy allows for a single actuated rotary joint to generate propulsive thrust forces and low resistive drag through a full sweep cycle. As such, its powered motion consists only of rotating back and forth about its root. The

[1]School of Mechanical & Aerospace Engineering Department, University of California, San Diego.
Contact e-mail ngravish @eng.ucsd.edu

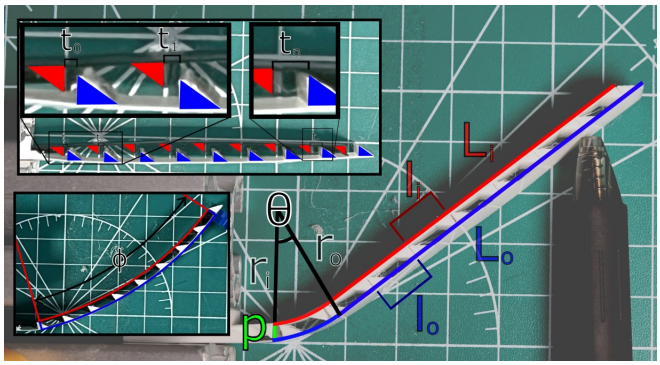

Fig. 1. Graphical representation of dimensions and variables of the straight JAMJam appendage, with $t_0 = 1$ and $c = 0$. The outer plate is shown in blue, and the inner plate is shown in red. The top inset shows the tooth separation variables t_i of the JAMJam appendage, and the bottom insert shows the additional curve ϕ of the curved appendage.

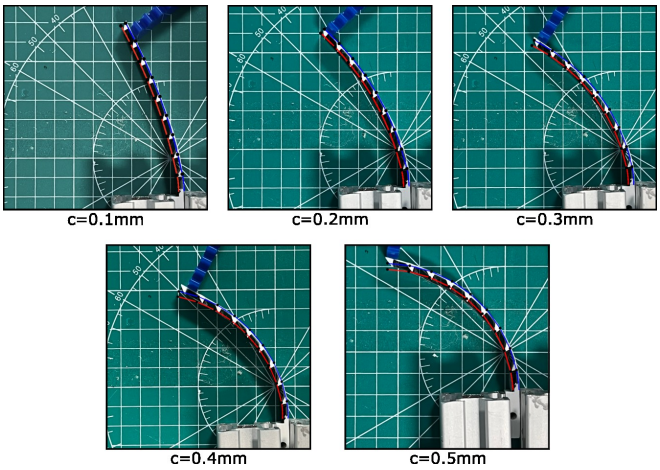

Fig. 2. Script-generated curve models for the curved appendage with estimations of tooth placement are compared to the actual appendages. The outer plate is in blue, the inner plate is in red, and the tooth placements are shown as black dots on the model.

anisotropic force generation results from its unique bending geometry.

The construction of the JAMJam appendage is based on previous manufacturing known as Flexoskeleton printing [25] [24]. This technique utilizes 3D printing a PLA plastic structure atop a thin sheet of polycarbonate (PC) plastic. The PC sheet adheres to the 3D printed structure, providing flexible thin plates with better elastic deformation than 3D printed parts alone. In the case that the PC does not adhere, super glue is applied to maintain adhesion. The 3D printers used to print the JAMJam appendages are a Prusa MK3 and Prusa Mini, FDM printers with high reliability and precision up to 0.05mm [26].

The JAMJam Appendage consists of two thin plates parallel at distance p to each other, constrained at the root of the appendage (Fig. 1). A small loose loop allows the plates to slide past each other but keep the two plates close together. The sides facing each other have teeth in a 3-4-5 right triangle configuration each spaced a distance l_o apart for the outer plate or l_i apart for the inner plate, as defined in Section II-A. The hypotenuses of the triangle teeth on the outer plate face away from the root of the appendage, whereas those on the inner plate face toward the root of the appendage.

As a result of the tooth geometry, during movement of the appendage, the teeth mesh together and jam only when the tip of the appendage experiences a force normal to the outer plate's toothed face. When the appendage is moving such that force is generated in the jamming direction, it is known as the 'step phase'. If the experienced force is directed normal to the outer plate's non-toothed face, then the appendage will not jam at any bend angle as the teeth will not mesh. When the appendage is moving in this manner, it is known as the 'swing phase' of the appendage.

A. Dimensions and Definitions

The JAMJam Appendage can be defined by the following parameters. Note the terms 'straight appendage' and 'curved appendage' will be defined in Sections II-B and II-C.

- n = A number to describe the position of a tooth on an appendage, starting from $n_{min} = 0$. For this paper, the maximum $n_{max} = 9$, really meaning there are 10 pairs of teeth on each appendage.
- l_o, l_i = Outer and inner plate tooth spacing, respectively.
- $L_o = n * l_o, L_i = n * l_i$ = Outer and inner plate total lengths, respectively. Dependent on l_o, l_i, and n.
- $p = r_o - r_i$ = Plate separation, the distance between the inner and outer plates of the appendage, as shown in Figure 1.
- t_0 = Initial tooth separation, the space between the inner and outer teeth that are closest to the root of the appendage, the 'root tooth pair,' as shown in Figure 1. For this paper, t_0 is tested from 1 mm to 4 mm in increments of 1 mm.
- $t_n = t_0 + c * n$ = Tooth separation at the n'th tooth from the root of the appendage when the appendage is free/unbent, as shown in Figure 1. Dependent on c, n, and t_0.
- $c = t_{n-1} - t_n$ = Difference in tooth separation from t_{n-1} to t_n when the appendage is free/unbent. For this paper, c is tested from 0 mm to 0.5 mm in increments of 0.1 mm with $t_0 = 1$mm.
- $\theta = t_0/p$ = Initial deflection angle of the appendage when bent in the jamming direction (which is also the 'total jammed deflection angle' for the straight appendage). Dependent on t_0 and p.
- $\phi = (c/p) * n$ = Curvature deflection angle of the appendage when bent in the jamming direction (which makes $\theta + \phi$ the total jammed deflection angle for the curved appendage). Dependent on c, p, and n.

B. Straight Appendage

The straight version of the JAMJam Appendage is defined as the appendage with $c = 0$, meaning that the initial tooth separation $t_0 = t_n$. When the straight appendage jams, it bends only at the first tooth closest to the root of the

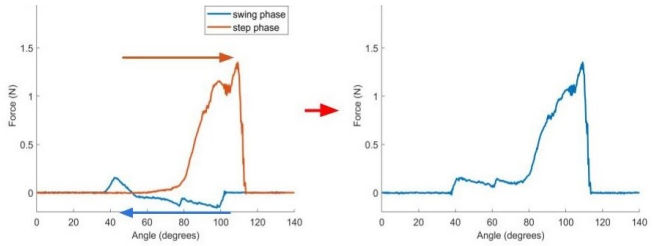

Fig. 3. Force data was collected for both the swing phase (blue) and step phase (orange) of the appendage's movement. It was then combined by flipping the swing phase data (to simulate an opposing appendage) and adding the force profiles together. The mean of 20 trials was taken for each set of variables tested.

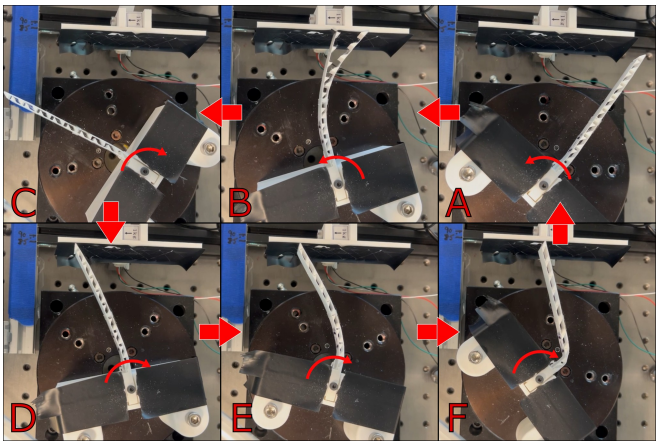

Fig. 4. An example of the motion of the traction experiment. Counter-clockwise from top right: A) The beginning of a cycle, the rotation stage moves counter-clockwise to begin the swing phase. B) The appendage bends out of the way in its swing phase. C) At the end of the swing phase, the appendage begins to be rotated clockwise to begin the step phase. D) First contact with the wall at the step phase. E) Initial jamming angle, at this point the appendage is jammed and imparts large force to the wall. F) In some instances, the appendage bends so much that it causes one sheet to buckle. After this, the appendage returns to its initial state A, ending the step phase.

appendage. This first bend forces the rest of the teeth to jam as well, as their separation is equal to the initial tooth separation, which goes to zero as the bend angle goes to its maximum. Figure 1 shows a straight appendage's shape when pushed in its jamming direction. In this paper, several variations of the initial tooth separation t_0, from 1mm to 4mm in increments of 1mm, are tested under the straight appendage model as discussed in Chapter III.

C. Curved Appendage

The curved version of the JAMJam Appendage is defined as the appendage with nonzero c. When the curved appendage jams, it first bends at the first tooth closest to the root of the appendage an amount dependent on t_0, similarly to the straight appendage. However, unlike the straight appendage, the other teeth do not jam immediately, as $t_n > t_0$. The teeth closest to the root jam next, and that continues down the appendage all the way to the tip, producing a curve dependent on the c, the rate of change in t_n. In this paper, several variations of c, from 0mm to 0.5mm in increments of 0.1mm, with $t_0 = 1$mm, are tested under the curved appendage model as discussed in Chapter III.

III. JAMJam Appendage Testing

The JAMJam Appendage's parameters were varied in the following manner. The parameters were chosen after initial prototyping of the appendage revealed the different angles at which the appendage would bend at, as explained in Section III-A.

- For the straight appendage ($c = 0$), the initial tooth separation t_0 was varied from 1mm to 4mm in increments of 1mm.
- For the curved appendage, the initial tooth separation t_0 was kept at 1mm, and c was varied from 0.1mm to 0.5mm in increments of 0.1mm.

A. Appendage Modeling

For the straight appendage, modeling its behavior consisted of bending each appendage until it jammed at its root tooth pair, which also jammed every other tooth pair. The deflection angle θ at which this bend occurred was measured (For reference, the main image in Figure 1 is an example of the deflection in the $t_0 = 1mm$ case). Each bend was conducted three times to determine some variance, which turned out to be relatively small. The relationship between t_0 and θ is determined to be linear. Initial tooth separation t_0 above 4mm was not tested because its jamming angle was too large to be usable for the purpose of locomotion.

For the curved appendage, modeling its behavior also consisted of bending each appendage, this time until it jammed at all of its tooth pairs, which generated a circular curve. This curve can be predicted using the variables given in Section II-A using the equations for the position of a circle $x = r_{[o,i]}\cos(\phi)$ and $y = r_{[o,i]}\sin(\phi)$ and the initial deflection angle θ. The resulting model curves with estimations of tooth placement are compared on top of the actual appendages as shown in Figure 2. Likewise to the straight appendage, change in tooth separation c was not tested above 0.5mm as its jamming angle was too large to be usable for the purpose of locomotion.

B. Traction Experiment Overview

The traction experiment aimed to understand the force profile of the JAMJam Appendage in direction of movement. The appendage was rotated on a rotation stage alternating between the swing phase and the step phase. The total angle that the appendage rotated in each direction, or total sweep, was 140 degrees. A wall segment attached to a force sensor was mounted at varying distances away from the appendage and rotation stage to simulate a surface that the appendage would traverse. The force sensor was attached to a LabJack and measured using an automated script during the entire step cycle of the appendage. The force sensor was directed such that the direction of the measured force was parallel to the wall, in effect measuring the shear friction force, or traction, between the appendage and the wall.

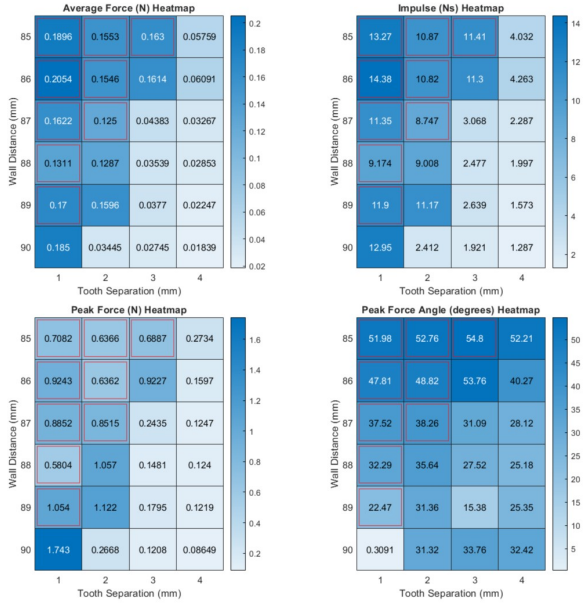

Fig. 5. Heatmap of mean force, impulse, peak force, and peak force angle for the straight appendage. Note: cases in which the appendage underwent significant plastic deformation are outlined in red.

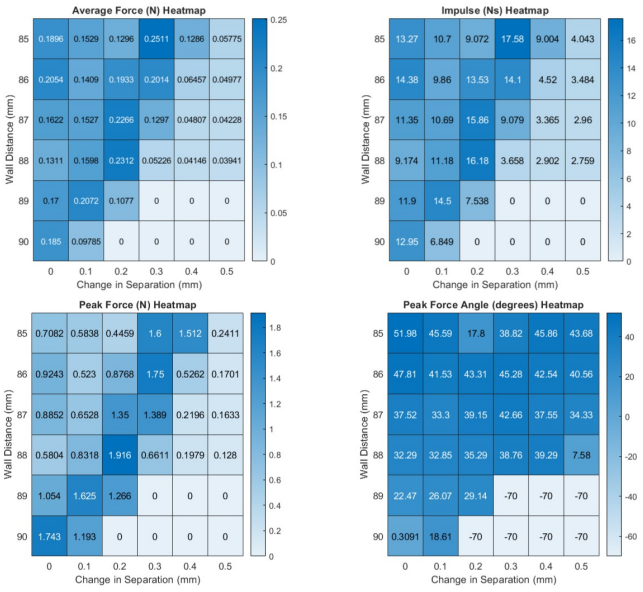

Fig. 6. Heatmap of mean force, impulse, peak force, and peak force angle for the curved appendage. Some cases were left untested and those are shown as zeros, or -70 in the case of the peak force angle.

The wall's distance from the center of rotation was varied from 85mm to 90mm in increments of 1mm. Each type and variant of appendage made 20 full step cycles (one swing phase and one step phase) against each wall distance. The force was measured over the entire cycle. See Figure 3 for an example of how force was measured, and then analyzed, to arrive at the following results.

In several cases of the straight appendage test, the appendage underwent undesired plastic deformation during the first or second step cycle. Figure 5 shows the cases in which this pre-deformation occurred, outlined in red.

Figure 5 depicts the average force, impulse, peak force, and peak force angle of the straight appendages tested for each wall distance. It can be seen that as the wall distance decreases, the optimal appendage t_0 increases. This is especially clear when considering that the pre-deformed cases outlined in red are not ideal and should be avoided, as even though they provide significant force, their lifespan is diminished from the initial buckling.

The impulse heatmap for the straight appendage confirms the findings from the average force heatmap. One appendage over its sweep can produce generous impulse for its size. Once again, while pre-deformed cases provide significant impulse, they should generally be avoided.

The peak force heatmap also confirms the previous findings. It should be noted that the smaller the wall distance, the smaller the achievable peak force by the straight appendage. This is due to the large deflection angle θ at which the $t_0 =$ 3mm and 4mm appendages jam at.

The peak force angle heatmap depicts the sweep angle at which the largest force occurs during the step phase of the appendage's movement. The angle informs how the appendage will behave on a robot platform. Generally, the peak force is immediately followed by the end of contact with the wall, and the appendage snaps back to its free position. This informs the minimum angle for which the appendage will complete a step cycle.

Figure 6 depicts the average force, impulse, peak force, and peak force angle of the curved appendages tested for each wall distance. It can be seen that as the wall distance decreases, the optimal appendage c increases. Compared to the straight appendage, the curved appendage has more flexibility, and the optimal appendages have larger magnitudes of average force than the optimal appendages of the straight variety.

The traction experiment showcases the abilities and shortcomings of different variants of the JAMJam Appendage for locomotion purposes. The straight appendage is best utilized with a low t_0 and has less tolerance for tight confines, but can still create good traction with a relatively small sweep if it is utilized in a suitable environment. The curved appendage has wider range of flexibility as any c tested can be used with success, and can be utilized in more confined spaces, however it requires the robot platform to have a much larger sweep angle capability which is not always feasible in simple systems. The robot designed for this paper could not accommodate extremely large sweep angles, and therefore the straight appendage was utilized. Further details will be discussed in Chapter IV.

IV. The JAMbot

The JAMJam Robot designed as shown in Figure 7 is designed to operate and explore in shallow water environments utilizing the passive compliance of the JAMJam Appendages.

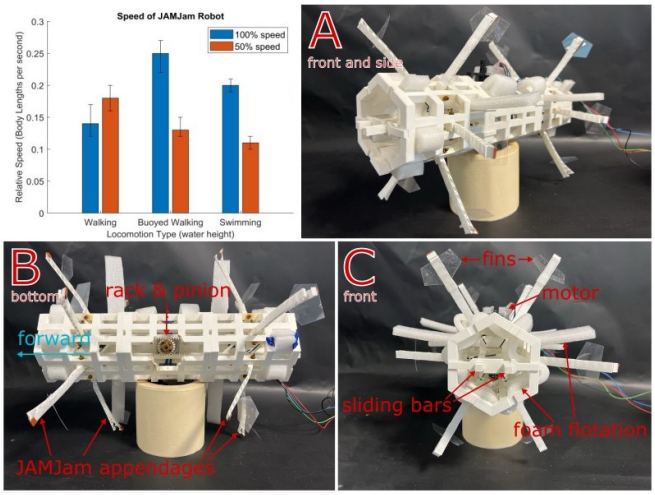

Fig. 7. The JAMJam Robot and associated speed plots in its three modes of movement. A) The robot's 'bow' and 'port side'. B) The robot's 'bottom', but the robot is considered invertible. Note the rack and pinion connected to the motor driving the sliding bars. C) The robot's 'bow', showing the sliding bars and the cross-section of the appendages.

A. Design and Development

The JAMJam Robot was conceived as a way to traverse difficult terrain, especially in environments where buoyancy could be achieved or where gravity was weak or nonexistent. It was also conceived as under-actuated, with minimizing the number of actuators as an objective. This could be achieved due to the passive flexibility and anisotropic capability of the JAMJam Appendage, which would allow it to traverse terrain without requiring sensors or complex actuation. The robot discussed in this paper is studied in a shallow-water environment, which could correlate to inter-tidal zones or even on the sea floor, as the robot could be made perfectly neutrally buoyant. To this end, appendages would have to protrude from all sides of the robot should it experience unwanted phenomena such as waves or curious sea life and become inverted. Thus the invertible tubular shape was proposed and prototyped into a long hexagonal prism.

The JAMJam Robot consists of two appendage sections and a motor section. The appendage sections are hexagonal prisms with one appendage on each of its six side faces, which are attached to two sliding bars inside the section. Each appendage moves in the opposite phase to the appendages closest to it. The motor section is also a hexagonal prism with a motor and rack and pinion mechanism to drive the sliding bars in the appendage sections. Other than the motor, no electronic components are on the robot, and thus it is essentially waterproof. Using a waterproof-rated motor would allow the robot to submerge completely. Each section is built to be modular, for different purposes more modules can be added if necessary. Each section has a length of 12 cm, making the robot have a total body length of 36 cm.

The JAMJam Robot is constructed from 3D printed PLA plastic parts using the same printers as the appendages, which are then glued together to make a solid structure. Each appendage is given a small plastic flipper to facilitate swimming. The appendages are attached to the robot using a single screw each, such that they are free to rotate. Carbon fiber rods are attached to each appendage, and each rod fits into a carefully positioned part of the sliding bars that provide motion for the appendages. The motor is then inserted into the motor section; in this robot, a standard stepper motor is used. It is controlled using position control and hosted on an Arduino board. Future work can be done to create an untethered version, so long as a battery is provided, and all electronics are waterproofed.

B. Locomotion Characteristics

The JAMJam Robot was determined to have three distinct modes of movement:

- **Walking** is considered to be the case in which the robot's bottom-pointing appendages are touching the ground for the majority of its step cycle, even though the robot is still somewhat supported by the buoyant force of the water. In this case the robot lifts itself a little out of the water during each step. The appendages touching the bottom often stay bent throughout the entire step cycle and do not reset to its pre-swing phase position as seen in Figure 8. During experimentation, it was found that having the water level below a certain point would prevent the robot from moving forward, because the distance between the appendage and the ground was too close together, as expected from the previous chapter's testing.
- **Buoyed Walking** is the case where the robot's bottom-pointing appendages are touching the ground only at the midpoint of its cycle and the buoyant force supports all of the weight of the robot. The tips of the bottom appendages make full cycles and reset each time.
- **Swimming** is the case where the robot's appendages do not touch the ground at all and is fully buoyed by water. The small fins on the ends of each appendage provide all of the forward force as the robot paddled.

Velocity tests were conducted in a test tank with a turf bottom. To test the different locomotive modes, the water height of the test tank was changed. The lowest water height that the robot would still have forward movement (the walking mode) was 15 cm. In all cases, the appendages which did not touch the ground or the sides of the test tank still provided some forward force with their fins pushing through the water. Figure 7 plots the velocities of the three different locomotive modes at 100% speed (actuating the appendages at 1.2 step cycles per second) and 50% speed. Each condition and motor speed was tested five times over two body lengths. The buoyed walking mode exhibited the fastest velocity when the motor was at 100% speed, followed closely by the swimming mode at 100% speed. The walking mode was generally faster at 50% speed than at 100%, however the walking mode also has large variations as the passive compliance of the appendages also induces randomness when walking on terrain.

The JAMJam robot was also tested in walking and swimming conditions with obstacles. Non-compliant obstacles

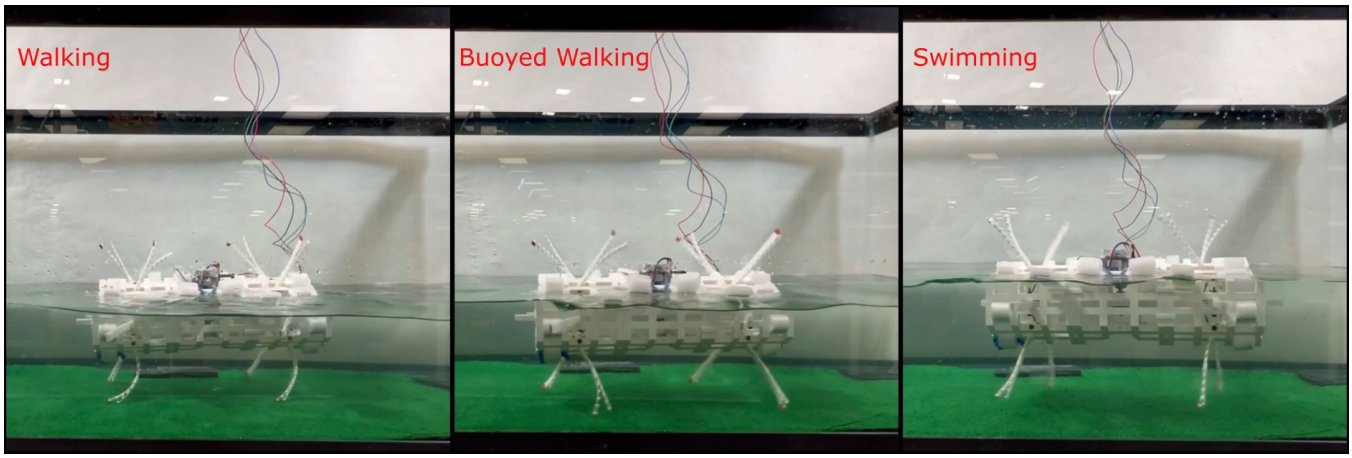

Fig. 8. The three different locomotive modes of the JAMJam Robot: Walking, Buoyed Walking, and Swimming. Note the bottom-pointing appendages in each condition. The walking condition appendages are almost always in contact with the ground. The buoyed walking condition appendages barely scrape the ground. The swimming condition appendages do not touch the ground.

such as small rocks stymied the swimming mode but were able to be traversed when in the buoyed walking mode. Compliant obstacles such as plastic kelp were able to be traversed over in the swimming mode and traversed around in the walking and buoyed walking modes.

V. Conclusion

In this paper the novel JAMJam Appendage was introduced for passively compliant, simply actuated locomotion. Design characteristics and variations were discussed. The appendage was tested for shear friction capability to determine its viability on a robot platform. The JAMJam Robot was introduced for shallow water locomotion with an emphasis on navigating inter-tidal zones and other coastal environments. Possible applications include exploration under sea ice, monitoring inter-tidal zones, and as a utility robot in coastal waters.

This paper created the first prototype of the JAMJam robot. While not explored in depth in this paper, improvements can be made to the appendage and the robot by adding some level of complexity. The JAMJam Appendage could be modified to include a way to change the tooth separation while on the robot, to change its properties, and therefore creating tunable anisotropy, depending on the conditions that the robot finds itself in. This could be done with shape memory alloy (SMA) actuators or a small worm gearing mechanism.

In this paper, the velocity of the robot in sand was not tested due to the difficulty of removing sand from a shared water tank. This should be done in order to compare the velocity and force generation of different strata. In addition, more study can be conducted on the effect of the ground-effect-like phenomena that occurred as the appendages swam close to the sandy bottom. This characterization could help to explain the large difference in swimming force generation between the turf and sand conditions.

The JAMJam Appendage could also be utilized for other applications. One possible idea is to create a gripper using two or three JAMJams. The gripper would be rigid in the direction of grip but flexible in the opposite direction, due to the anisotropic nature of the appendage. Only a single motor would be needed to actuate the gripper as a result, and it would be more compliant than traditional grippers.

Another JAMJam robot could be created to traverse dry terrain if given stiffer appendages, or lower total weight. A possible concept is to explore undersea ice inaccessible to wheeled robots with positive buoyancy [27]. A robot system utilizing JAMJam Appendages could also be designed for extra-terrestrial missions in low- or micro-gravity environments. Such robot systems would ideally be equally or more invertible than the JAMJam robot presented in this paper. Lastly, different sizes of JAMJam robot can be constructed to determine their feasibility for locomotion.

Acknowledgments

Funding support was provided through the Mechanical and Aerospace Engineering Department at UCSD. This material is based upon work supported by the National Science Foundation under Grant No. 1935324 and the Office of Naval Research under grant number N00014-20-1-2373. Any opinions, findings, and conclusions or recommendations expressed in this material are those of the author(s) and do not necessarily reflect the views of the National Science Foundation or ONR.

References

[1] L. Bruzzone and G. Quaglia, "Review article: locomotion systems for ground mobile robots in unstructured environments," *Mechanical Sciences*, vol. 3, no. 2, pp. 49–62, 2012. [Online]. Available: https://ms.copernicus.org/articles/3/49/2012/

[2] C. Laschi, B. Mazzolai, and M. Cianchetti, "Soft robotics: Technologies and systems pushing the boundaries of robot abilities," *Science Robotics*, vol. 1, no. 1, p. eaah3690, 2016. [Online]. Available: https://www.science.org/doi/abs/10.1126/scirobotics.aah3690

[3] J. Faigl and P. Čížek, "Adaptive locomotion control of hexapod walking robot for traversing rough terrains with position feedback only," *Robotics and Autonomous Systems*, vol. 116, pp. 136–147, 2019. [Online]. Available: https://www.sciencedirect.com/science/article/pii/S0921889018306614

[4] S. G. Desai, A. R. Annigeri, and A. TimmanaGouda, "Analysis of a new single degree-of-freedom eight link leg mechanism for walking machine," *Mechanism and Machine Theory*, vol. 140, pp. 747–764, 2019. [Online]. Available: https://www.sciencedirect.com/science/article/pii/S0094114X19309097

[5] *A Miniature, 3D-Printed, Walking Robot With Soft Joints*, ser. International Design Engineering Technical Conferences and Computers and Information in Engineering Conference, vol. Volume 5B: 41st Mechanisms and Robotics Conference, 08 2017. [Online]. Available: https://doi.org/10.1115/DETC2017-68182

[6] W. Gronenberg, "Fast actions in small animals: Springs and click mechanisms," *Journal of Comparative Physiology*, vol. 178, pp. 727–734, 06 1996.

[7] K. Jayaram and R. J. Full, "Cockroaches traverse crevices, crawl rapidly in confined spaces, and inspire a soft, legged robot," *Proceedings of the National Academy of Sciences*, vol. 113, no. 8, pp. E950–E957, 2016. [Online]. Available: https://www.pnas.org/doi/abs/10.1073/pnas.1514591113

[8] S. Kim, J. E. Clark, and M. R. Cutkosky, "isprawl: Design and tuning for high-speed autonomous open-loop running," *The International Journal of Robotics Research*, vol. 25, no. 9, pp. 903–912, 2006. [Online]. Available: https://doi.org/10.1177/0278364906069150

[9] M. Calisti, F. Corucci, A. Arienti, and C. Laschi, "Dynamics of underwater legged locomotion: Modeling and experiments on an octopus-inspired robot," *Bioinspiration & Biomimetics*, vol. Bioinspir. Biomim. 10 (2015) 046012., 07 2015.

[10] T. Ranzani, G. Gerboni, M. Cianchetti, and A. Menciassi, "A bioinspired soft manipulator for minimally invasive surgery," *Bioinspiration & Biomimetics*, vol. 10, no. 3, p. 035008, may 2015. [Online]. Available: https://dx.doi.org/10.1088/1748-3190/10/3/035008

[11] C. M. Wheeler and M. L. Culpepper, "Soft Origami: Classification, Constraint, and Actuation of Highly Compliant Origami Structures," *Journal of Mechanisms and Robotics*, vol. 8, no. 5, p. 051012, 05 2016. [Online]. Available: https://doi.org/10.1115/1.4032472

[12] H.-T. Lin, G. Leisk, and B. Trimmer, "Goqbot: A caterpillar-inspired soft-bodied rolling robot," *Bioinspiration & Biomimetics*, vol. 6, p. 026007, 06 2011.

[13] A. Arienti, M. Calisti, F. Giorgio Serchi, and C. Laschi, "Poseidrone: Design of a soft-bodied rov with crawling, swimming and manipulation ability," 09 2013.

[14] X. Huang, K. Kumar, M. K. Jawed, A. M. Nasab, Z. Ye, W. Shan, and C. Majidi, "Chasing biomimetic locomotion speeds: Creating untethered soft robots with shape memory alloy actuators," *Science Robotics*, vol. 3, no. 25, p. eaau7557, 2018. [Online]. Available: https://www.science.org/doi/abs/10.1126/scirobotics.aau7557

[15] E. Lathrop, M. T. Tolley, and N. Gravish, "Directionally compliant legs enabling crevasse traversal in small ground-based robots," *Advanced Intelligent Systems*, vol. 5, no. 4, p. 2200258, 2023. [Online]. Available: https://onlinelibrary.wiley.com/doi/abs/10.1002/aisy.202200258

[16] H. Chang, J. Chang, G. Clifton, and N. Gravish, "Anisotropic compliance of robot legs improves recovery from swing-phase collisions," *Bioinspiration & Biomimetics*, vol. 16, no. 5, p. 056001, aug 2021. [Online]. Available: https://dx.doi.org/10.1088/1748-3190/ac0b99

[17] B. Aktaş and R. D. Howe, "Tunable anisotropic stiffness with square fiber jamming," in *2020 3rd IEEE International Conference on Soft Robotics (RoboSoft)*, 2020, pp. 879–884.

[18] Y. Ozkan-Aydin, B. Chong, E. Aydin, and D. I. Goldman, "A systematic approach to creating terrain-capable hybrid soft/hard myriapod robots," in *2020 3rd IEEE International Conference on Soft Robotics (RoboSoft)*, 2020, pp. 156–163.

[19] A. Rafsanjani, Y. Zhang, B. Liu, S. M. Rubinstein, and K. Bertoldi, "Kirigami skins make a simple soft actuator crawl," *Science Robotics*, vol. 3, no. 15, p. eaar7555, 2018. [Online]. Available: https://www.science.org/doi/abs/10.1126/scirobotics.aar7555

[20] S. Chopra, D. Vasile, S. Jadhav, M. Tolley, and N. Gravish, "Toward robotic sensing and swimming in granular environments using underactuated appendages," *Advanced Intelligent Systems*, vol. 5, 05 2023.

[21] R. Olfati-Saber and A. Megretski, "Nonlinear control of underactuated mechanical systems with application to robotics and aerospace vehicles," Ph.D. dissertation, USA, 2001, aAI0803036.

[22] O. Kanner and A. Dollar, "Kinematic design of an underactuated robot leg for passive terrain adaptability and stability," *Journal of Mechanisms and Robotics*, vol. 5, p. 031006, 08 2013.

[23] R. Ozawa, K. Hashirii, and H. Kobayashi, "Design and control of underactuated tendon-driven mechanisms," in *2009 IEEE International Conference on Robotics and Automation*, 2009, pp. 1522–1527.

[24] M. Jiang, Z. Zhou, and N. Gravish, "Flexoskeleton printing enables versatile fabrication of hybrid soft and rigid robots," *Soft Robotics*, vol. 7, 04 2020.

[25] Q. Yu, M. Jiang, and N. Gravish, "Flexoskeleton fingers: 3d printed reconfigurable ridges enabling multi-functional and low-cost underactuated grasping," *IEEE Robotics and Automation Letters*, vol. PP, pp. 1–1, 03 2021.

[26] 2023. [Online]. Available: https://help.prusa3d.com/

[27] J. Leichty, A. T. Klesh, D. F. Berisford, J. B. Matthews, and K. P. Hand, "Positive-buoyancy rover for under ice mobility," 2013. [Online]. Available: https://api.semanticscholar.org/CorpusID:127948044